JGR Oceans

RESEARCH ARTICLE

10.1029/2024JC021222

Water Mass Transformation and Its Relationship With the Overturning Circulation in the Eastern Subpolar North Atlantic

Yao Fu[1], **M. Susan Lozier**[1], **Sudip Majumder**[1], **and Tillys Petit**[2]

[1]Georgia Institute of Technology, Atlanta, GA, USA, [2]National Oceanography Centre, Southampton, UK

Abstract A recent study using the first 21 months of the OSNAP time series revealed that the export of dense waters in the eastern subpolar North Atlantic——as part of the Atlantic Meridional Overturning Circulation (MOC)——can be almost wholly attributed to surface-forced water mass transformation (SFWMT) in the Irminger and Iceland basins, thus suggesting a minor role for other means of transformation, such as diapycnal mixing. To understand whether this result is valid over a period that exceeds the current observational record, we use four different ocean reanalysis products to investigate the relationship between surface buoyancy forcing and dense water production in this region. We also reexplore this relationship with the now available 6-year OSNAP time series. Our analysis finds that although surface transformation in the eastern subpolar gyre dominates the production of deep waters, mixing processes downstream of the Greenland Scotland Ridge are also responsible for the production of waters carried within the AMOC's lower limb both in the observations and reanalyses. Further analysis of the reanalyses shows that SFWMT partly explains MOC interannual variability, the remaining portion can be attributed to basin storage and mixing. Compared to the observations, the reanalyses exhibit stronger MOC variance but comparable SFWMT variance on interannual timescales.

Plain Language Summary The transformation of water masses from lighter to denser density classes due to surface heat and freshwater fluxes is considered as a major source of sustaining the lower limb of the Atlantic Meridional Overturning Circulation (MOC). In this study, we quantify the relationship between surface-forced water mass transformation and the MOC in the mean state and on seasonal and interannual timescales using ocean observations and data assimilation products. We find that surface-forced water mass transformation is responsible for a large portion of the time-mean MOC lower-limb transport, and it can partly explain MOC interannual variability, highlighting the important role of surface-forced water mass transformation to the MOC in the mean and variability.

Key Points:

- Surface-forced water mass transformation (SFWMT) explains a large portion of the mean meridional overturning circulation (MOC) in the eastern subpolar North Atlantic
- MOC interannual variability can be partly explained by SFWMT variability
- Ocean reanalysis products show stronger MOC variance but comparable SFWMT variance on interannual timescales compared to the observations

Supporting Information:

Supporting Information may be found in the online version of this article.

Correspondence to:

Y. Fu,
yaofu@gatech.edu

Citation:

Fu, Y., Lozier, M. S., Majumder, S., & Petit, T. (2024). Water mass transformation and its relationship with the overturning circulation in the eastern subpolar North Atlantic. *Journal of Geophysical Research: Oceans*, *129*, e2024JC021222. https://doi.org/10.1029/2024JC021222

Received 15 APR 2024
Accepted 2 DEC 2024

Author Contributions:

Conceptualization: Yao Fu, M. Susan Lozier, Sudip Majumder
Formal analysis: Yao Fu
Funding acquisition: M. Susan Lozier
Methodology: Sudip Majumder, Tillys Petit
Supervision: M. Susan Lozier
Visualization: Yao Fu
Writing – original draft: Yao Fu
Writing – review & editing: Yao Fu, M. Susan Lozier, Sudip Majumder, Tillys Petit

1. Introduction

The Atlantic Meridional Overturning Circulation (MOC) redistributes heat and freshwater on a global scale, making it a critical component of the Earth's climate system. A large portion of the waters constituting the lower AMOC limb are formed in the subpolar North Atlantic (SPNA, Rhein et al., 2011). Warm and saline waters of subtropical origin, advected into the SPNA by the MOC upper limb, are cooled through contact with the atmosphere, resulting in densification and sinking of the surface waters. The process of transforming light surface water into dense deep water due to surface buoyancy fluxes is referred to as surface-forced water mass transformation (SFWMT).

Past studies have suggested that SFWMT is a major contributor to the volume transport of the MOC lower limb. Desbruyères et al. (2019) suggest that SFWMT north of 45°N is a predictor of the MOC at 45°N with a lead time of 5 years, whereas Isachsen et al. (2007) and Årthun (2023) show that SFWMT explains the mean and variability of the overturning circulation in the Nordic Seas. Buckley et al. (2023) further showed using ECCO data that the mean MOC at 45°N matches well with the mean SFWMT in the SPNA. Finally, an analysis of state-of-the-art climate models finds that models with higher mean SFWMT generally have a stronger mean MOC (Jackson & Petit, 2023).

Although an observation-based study has suggested a strong linkage between SFWMT and the MOC in the SPNA (Desbruyères et al., 2019), a direct attribution has not been possible due to the lack of a direct measurement of the SPNA overturning. The advent of the Overturning in the Subpolar North Atlantic Program (OSNAP; Lozier

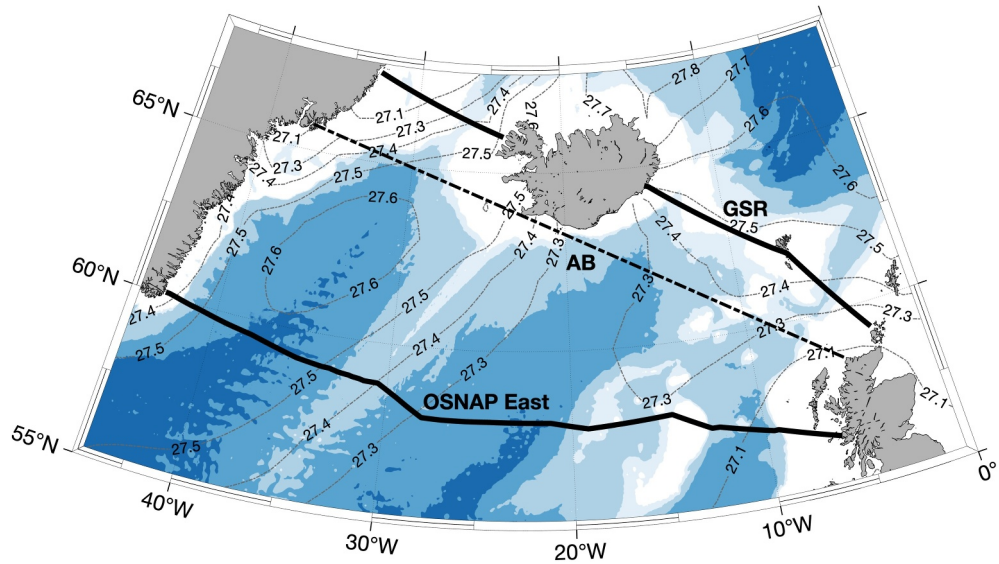

Figure 1. Map of the eastern subpolar North Atlantic. The OSNAP East, Greenland-Scotland Ridge (GSR), and AB sections are indicated on the map. The dashed contours with labels indicate climatological winter sea surface potential density estimated from EN4. The shading indicates ocean bottom depths at 500, 1,000, 2,000, and 3,000 m. Areas with water depth shallower than 500 m are shaded white.

et al., 2017) has allowed for that attribution by providing a direct measure of the MOC across the SPNA (Li et al., 2021; Lozier et al., 2019). Using a combination of moored instruments, Argo floats, satellite altimetry, and ship measurements (Lozier et al., 2017), OSNAP has produced 6 years of continuous observations since 2014 (Fu et al., 2023a; Li et al., 2021; Lozier et al., 2019). Using the first 2 years of OSNAP observations, Lozier et al. (2019) showed that overturning in the eastern SPNA dominates the mean and variability of the total subpolar MOC, with overturning in the Labrador Sea playing a minor role. This result has been confirmed by subsequent OSNAP observations to date (Fu et al., 2023a; Li et al., 2021). Furthermore, in an investigation of the seasonality of the subpolar MOC using the 6-year OSNAP observations, Fu et al. (2023a) found that SFWMT in winter precedes the spring MOC peak by a few months, a relationship that suggests causality consistent with the results and interpretation of Le Bras et al. (2020).

Using the then-available first 21 months of OSNAP observations (August 2014 to April 2016), Petit et al. (2020) demonstrated that the time-mean transport divergence in the overturning's lower limb in the eastern SPNA can be almost entirely explained by the time-mean SFWMT over that period. In contrast, Evans et al. (2023) found that SFWMT alone cannot account for the total time-mean MOC at OSNAP and that mixing-induced transformation is required to fill the gap. The short observational period used by Petit et al. (2020) raised the obvious question as to the representativeness of this relationship on longer timescales. To answer this question, we use the now-available 6-year OSNAP observations and (to focus on even longer time scales) ocean reanalysis products to investigate the relationship between SFWMT and the MOC.

We focus our study on the eastern SPNA (Figure 1) between OSNAP East and the Greenland-Scotland Ridge (GSR). We utilize available observations at the two sections and four different ocean reanalysis products (hereafter reanalysis) to investigate the contribution of SFWMT to the MOC's lower limb in the mean and on seasonal and interannual timescales. As part of our study, we assess the ability of the ocean reanalyses to simulate the observed SFWMT and MOC in the eastern SPNA over these timescales.

2. Data and Methods

In this section, we introduce the observations and reanalyses used in our study and then describe the calculation methods for the MOC lower limb transports, SFWMT, and lower limb volume budget.

Table 1
Information on the Four Ocean Reanalyses Used in This Study

Reanalyses	Time period	Spatial/Temporal resolution	Forcing	Base model	Assimilated data
ECCOv4r4	1992–2017	0.5 deg, 50 depth levels, monthly	ERA-Interim	MITgcm	In situ T/S profiles, SST, altimetry sea level, ice cover
GloSea5	1993–2020	0.25 deg, 75 depth levels, monthly	ERA-Interim	NEMO	In situ T/S profiles, SST, altimetry sea level, ice concentration
CGLORS	1993–2020	0.25 deg, 75 depth levels, monthly	ERA-Interim	NEMO	In situ T/S profiles, SST, altimetry sea level, ice concentration
SODA3.15.2	1980–2020	0.5 deg, 50 depth levels, monthly	ERA5	MOM5	In situ T/S profiles, SST

2.1. Ocean Observations

The OSNAP East section, which stretches from the southern tip of Greenland to the Scottish shelf (Lozier et al., 2017) provides continuous measurements of the meridional volume, heat, and freshwater transports in the eastern SPNA. We use the gridded monthly fields of velocity, temperature, and salinity across OSNAP East (Fu et al., 2023b) to calculate MOC lower limb transports across this section. The monthly gridded data fields have a horizontal resolution of ∼25 km, a vertical resolution of 20 m, and cover a time period from August 2014 to June 2020. An additional month of data in July 2020 is included in this study using the recovered OSNAP mooring data in 2022 in order to have a complete 6 years of OSNAP observations. The MOC lower limb is defined as the total transport below the time-mean σ_{MOC}, which is defined as the isopycnal of the maximum time-mean overturning streamfunction in density coordinates, following Lozier et al. (2019).

The GSR section consists of the Denmark Strait, the Iceland-Faroe Ridge, the Faroe Bank Channel, and the Wyville-Thomson Ridge (Bringedal et al., 2018). The southward transport of overflow waters is primarily through the Denmark Strait and the Faroe-Bank Channel. The mean Denmark Strait Overflow Water transport is reported to be 3.2 Sv in the period of 1996–2016 (Jochumsen et al., 2017). The mean overflow water transport through the Faroe Bank Channel is reported to be 2.2 Sv in the period of 1995–2015 (Hansen et al., 2016). The overflow water transports through the Iceland-Faroe Ridge (0.4 Sv, Hansen et al., 2018) and Wyville-Thomson Ridge (0.8 Sv, Sherwin et al., 2008) are relatively weak. In this study, we use a mean transport of 6.6 Sv for the mean lower limb transport across the GSR section, as it is the sum of the transports reported by the studies mentioned above. We compute the transport variance estimates at GSR (see Section 3.4) using the overflow transport time series at Denmark Strait and Faroe Bank Channel as they offer the longest observational record from 1996 to 2015 (Bringedal et al., 2018).

2.2. Ocean Reanalyses

We use four ocean reanalyses: (a) ECCO version 4 release 4 (hereafter ECCO, Estimating the Circulation and Climate of the Ocean, Forget et al., 2015; Wunsch & Heimbach, 2006), (b) UK Met Office GloSea5 (Global Seasonal Forecasting System version 5, Maclachlan et al., 2015), (c) CGLORS (CMCC Global Ocean Physical Reanalysis System; Storto et al., 2016), and (d) SODA version 3.15.2 (Simple Ocean Data Assimilation, Carton et al., 2018). Among the four products, ECCO is a dynamically consistent ocean state estimate that uses the adjoint method to bring the simulation close to observations (Forget et al., 2015). GloSea5 and CGLORS use 3DVar schemes (NEMOVAR and OceanVar, respectively) to assimilate observation data. SODA uses a sequential approach for the assimilation. The temporal coverage, spatial resolution, atmospheric forcing, base ocean model, and assimilated data for these reanalyses are listed in Table 1. Please refer to the corresponding publications listed above for further details of each reanalysis. We selected these ocean reanalyses because we have determined that they (a) have overturning structure and magnitude that compare favorably to those from the OSNAP observations and (b) have realistic SFWMT throughout the density range of the eastern SPNA compared to observations (Figure 2, see Section 3.1 for detail). Note that these ocean reanalyses have other shortcomings, for example, compared to the observations ECCO overestimates the overturning in the Labrador Sea, while it underestimates the overflow water transports across OSNAP East (Han, 2023). For a comprehensive investigation of the ocean reanalyses, please refer to Jackson et al. (2019).

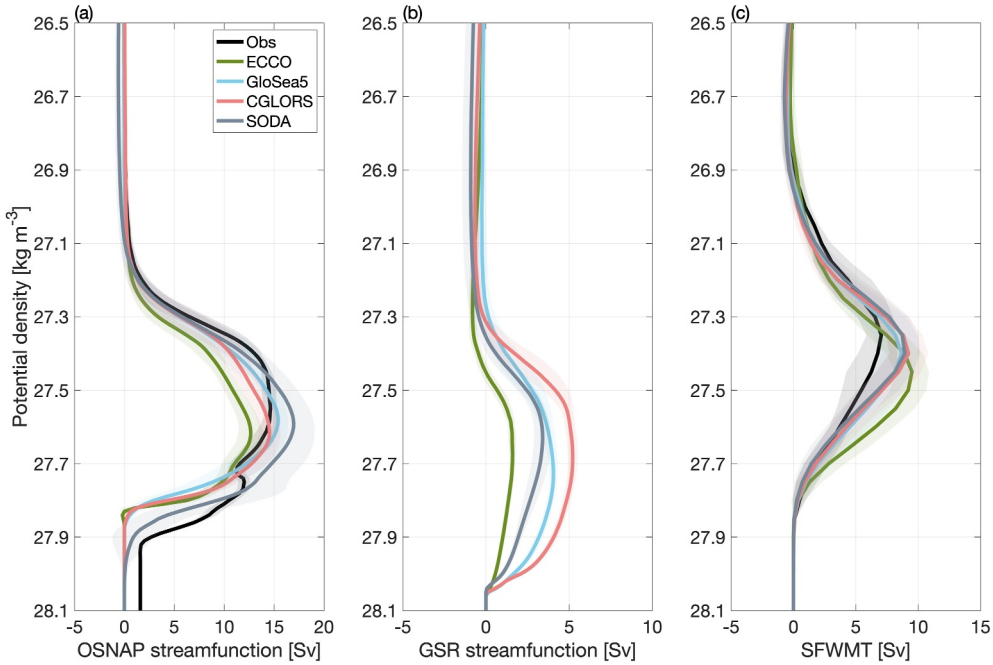

Figure 2. Overturning streamfunction in density coordinates at OSNAP East (a) and GSR (b), and surface-forced water mass transformation (SFWMT) between GSR and OSNAP East over the same density range (c) based on observations and four ocean reanalyses. The shading indicates the standard deviation estimated from the annual mean streamfunction and transformation time series. The SFWMT calculated based on the density field derived from EN4 is referred to as observation (black), and those from the density fields of the four ocean reanalyses are color-coded.

2.3. Reanalysis-Based Volume Transport Calculation

For the reanalyses used in this study, we estimate the lower limb volume transports across OSNAP East, GSR, and the "AB" section (Figure 1). The AB section, located ~300 km south of the GSR line, is used to examine the lower limb volume transport downstream from the GSR section. Temperature, salinity, and velocity data are extracted at all three sections from the original reanalysis grid to a new grid with 0.25° horizontal resolution and 20 m vertical resolution using a shape-preserving piecewise cubic interpolation method. The zonal and meridional velocity fields are then horizontally rotated to obtain a velocity field that is perpendicular to each section.

We first calculate the overturning streamfunction at OSNAP East in density coordinates following Lozier et al. (2019). We then determine the time-mean isopycnal of the maximum overturning streamfunction (σ_{MOC}) at OSNAP East. Finally, we calculate the volume transport below the time-mean σ_{MOC} at each section and refer to this as the lower limb transport. To facilitate the computation of the lower limb volume budget (descried in Section 2.5), a zero net transport constraint across each section is imposed to the ocean reanalysis data by applying a uniform compensating velocity across the entire section. The resultant time-mean compensating transports (i.e., by integrating the compensating velocity over the section) for ECCO, GloSea5, CGLORS, and SODA are 0.3, −0.4, −2.0, and −1.0 Sv, respectively. This zero-transport constraint is slightly different from that used for the OSNAP observations, where a 1.6 Sv net flow across OSNAP East is imposed to accommodate inflow from Davis Straits across OSNAP West (see Lozier et al., 2019). A sensitivity test using the OSNAP observations found a negligible difference for the overturning streamfunction and the MOC whether 0 or 1.6 Sv net flow is applied.

2.4. Surface-Forced Water Mass Transformation

The transformation of surface water by surface buoyancy fluxes at a density outcrop σ^* is estimated using a linearized equation of state (Speer & Tziperman, 1992) as

$$SFWMT(\sigma^*) = \frac{1}{\Delta\sigma}\iint SBF\ \Pi(\sigma)\, dx\, dy \quad (1)$$

$$SBF = -\frac{\alpha}{C_p}Q_{net} + \beta\frac{S}{1-S}(E-P) \quad (2)$$

where $\Pi(\sigma) = 1$ for $|\sigma - \sigma^*| \leq \frac{\Delta\sigma}{2}$ and $\Pi(\sigma) = 0$ elsewhere. α, β, C_p, Q_{net}, E, P, S, and SBF are the thermal expansion coefficient, haline contraction coefficient, specific heat of water, net heat flux, evaporation, precipitation, sea surface salinity, and surface buoyancy flux, respectively. Note that the unit of E and P is converted to kg m^{-2} s^{-1} before calculating SFWMT.

A monthly time series of SFWMT is calculated for the density bin between $\sigma_{MOC} \pm \frac{\Delta\sigma}{2}$ over the area bracketed by OSNAP East and GSR. This calculation is repeated over the area bracketed by OSNAP East and the AB section (Figure 1). We use the time-mean σ_{MOC} at OSNAP East for both calculations. Using a time-varying σ_{MOC} has a marginal impact on the calculated SFWMT. Following Petit et al. (2020), we select the size of the density bin, $\Delta\sigma$, as 0.2 kg m^{-3} in the eastern SPNA region for the observations and the reanalyses. The surface density fields are derived from the temperature (T) and salinity (S) at the shallowest depth level (5 m) from EN4.2.2 (Good et al., 2013) for the observation-based estimates and from the T/S fields for the reanalysis-based estimates.

Among the four ocean reanalyses, ECCO provides not only the temperature, salinity and velocity fields but also dynamically consistent surface forcing fields (e.g., heat and freshwater fluxes). Therefore, for the ECCO-based SWMWT calculation, we use its T/S fields combined with its own heat and freshwater fluxes. The other three reanalyses do not provide their heat and freshwater fluxes. The surface fluxes are typically subjected to large uncertainty (Jackson et al., 2019). To account for the lack of consistency in the surface heat and freshwater fields, we average the monthly surface heat and freshwater fluxes from three different sources: European Center for Medium-Range Weather Forecasts Reanalysis 5 (ERA5) atmospheric reanalysis (Poli et al., 2016); National Centers for Environmental Predictions Climate Forecast System Reanalysis (NCEP; Kanamitsu et al., 2002); and ECCOv4r4. We apply these averaged fluxes to the surface T/S fields of the observations and of the three reanalyses. In addition, we calculate different estimates of SFWMT by applying each of the surface fluxes to the observed density field as well as GloSea5, CGLORS, and SODA density fields. These estimates reveal the sensitivity of SFWMT to the different flux fields. A recent study also found that the temporal resolution of the surface flux field may have substantial impact on the SFWMT, that is, using daily heat and freshwater fields resulted in a weaker SFWMT compared to the estimates using weekly data (Stendardo et al., 2024). A future study will be needed to quantify the impact of different temporal resolutions of the forcing fields (e.g., subdaily or monthly) on the magnitude and variability of SFWMT for different regions.

2.5. Reanalysis-Based Lower Limb Volume Budget

To understand the role of surface transformation in driving MOC interannual variability, we calculate a volume budget for the lower limb in the enclosed area between GSR and OSNAP East (Figure 1) for all reanalyses:

$$\frac{dVol}{dt} = SFWMT - \nabla \cdot V + R \quad (3)$$

where Vol is the volume of water denser than σ_{MOC}. Vol is calculated by integrating the thickness between σ_{MOC} and ocean bottom over the enclosed area between GSR and OSNAP East. Equation 3 states that the lower limb volume change, $\frac{dVol}{dt}$, results from SFWMT, the transport difference between OSNAP East and GSR, and other processes (R). Note that although the lower limb transport at OSNAP East and at GSR are southward, the former is of larger magnitude than the latter. Therefore, $-\nabla \cdot V$ in Equation 3 is negative, representing a transport divergence that acts to decrease the volume. We assume that R includes processes such as diapycnal transformation across steep isopycnal slopes due to lateral diffusive fluxes (Marshall et al., 1999), entrainment at the base of the mixed layer and by the overflow waters (Hansen et al., 2016; Jochumsen et al., 2015) and/or processes such as cabbeling and frontogenetic strain at thermohaline fronts (Thomas & Shakespeare, 2015). In addition to these processes, R is also understood to include any spurious diapycnal mixing related to model formulation.

The volume budget is repeated for the area between OSNAP East and AB (Figure 1) to investigate the relative contribution of R downstream away from the GSR, where the overflow waters spill over the Ridge and, thus, where transformation due to mixing is expected to be most prevalent. Note that the lower limb transport across

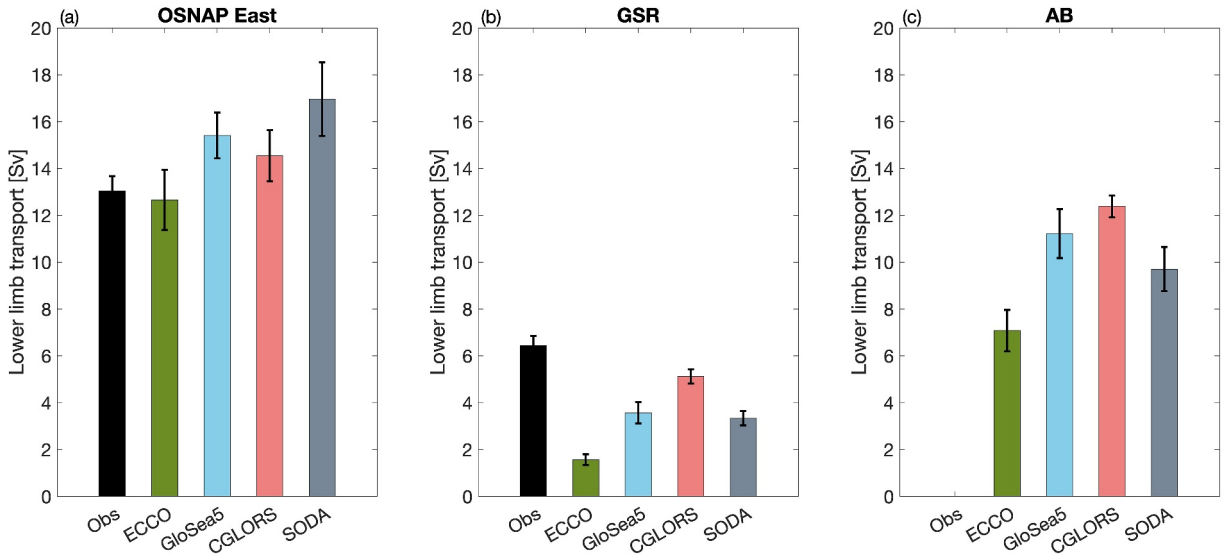

Figure 3. Time-mean transport across the (a) OSNAP East, (b) GSR, (c) AB sections based on the observations and reanalyses. The error bars represent the standard deviation estimated from the annual mean time series.

GSR and AB are determined as the transport below the σ_{MOC} of OSNAP East in each reanalysis. Over the full period of each reanalysis, the mean volume change, $\frac{\overline{dVol}}{dt}$, equals approximately 0 (around ±0.1 Sv for all reanalyses). Therefore, for the mean volume budget, Equation 3 becomes:

$$\nabla \cdot V = SFWMT + R \tag{4}$$

Note that the lower limb volume budget is only calculated using the reanalysis data, as they provide complete sections of temperature, salinity, and velocity at the OSNAP, GSR, and AB sections, which are not fully available for the observations.

3. Results

3.1. Mean Volume Budget

In this section, we first evaluate the performance of the selected reanalyses in simulating the mean MOC at OSNAP East and transformation in the eastern SPNA. We then investigate the mean-state relationship between SFWMT and the lower limb divergence through volume budget estimates.

The four ocean reanalyses generally produce a mean overturning circulation in potential density coordinates at OSNAP East (Figure 2a) that is consistent with the OSNAP observations. The northward flow in the upper limb starts to accumulate from ~27.1 kg m^{-3} and reaches a maximum at about 27.6 kg m^{-3} below which the southward returning flow completes the overturning.

We next compare the SFWMT over the same density range as the overturning streamfunction (Figure 2c). Overall, the reanalyses capture the observed structure and strength of SFWMT. Three out of four reanalyses have an SFWMT peak at ~ 27.4 kg m^{-3}, which agrees well with the observations. ECCO shows the SFWMT peak at a slightly higher density (27.5 kg m^{-3}). Compared to the overturning streamfunction, the SFWMT maximum occurs at lighter isopycnals for the observations and for the reanalyses and its magnitude is weaker than the overturning maximum in all cases. Both features suggest that other processes (e.g., mixing) contribute to the densification of the water from the peak SFWMT density.

We next examine the time-mean lower limb transports across the OSNAP East, GSR, and AB sections (Figure 3), but first note that at OSNAP East, the lower limb transport is equivalent to the MOC strength (maximum of the overturning streamfunction). The mean MOC from the reanalyses ranges from 12.7 ± 2.3 Sv (ECCO) to 17.0 ± 3.5 Sv (SODA). All estimates agree with the observed mean MOC (14.6 ± 3.0 Sv at 27.55 kg m^{-3}) within

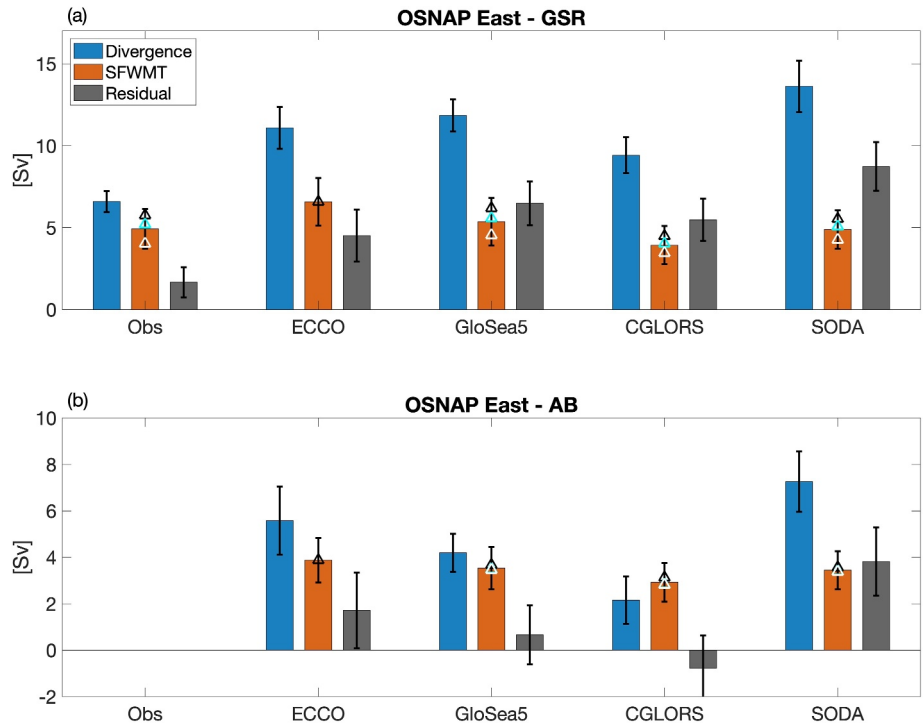

Figure 4. Time-mean budget of the lower limb volume between (a) the OSNAP East and GSR sections and (b) the OSNAP East and AB sections. The error bars represent the standard deviation estimated from the annual mean time series. For SFWMT, the red bar is estimated using the merged surface forcing fields from ECCO, ERA5, and NCEP. The triangles represent the estimates based on single-source forcing fields (ECCO in black, ERA5 in cyan, NCEP in white, see Section 2.4).

the uncertainty. In contrast, all mean lower limb transport from the reanalyses at the GSR section are weaker than the observations, which is 6.5 ± 0.4 Sv. ECCO has the weakest GSR transport (1.6 ± 0.2 Sv) among the four products, whereas CGLORS has the strongest (5.1 ± 0.3 Sv), making it more in line with the observations. At the AB section (where there are no observations available for comparison), all reanalyses show a substantially enhanced lower limb transport downstream from the GSR section. The AB transports follow a similar pattern as the GSR transports with ECCO showing the weakest AB transport and CGLORS showing the strongest transport.

Following Equation 4, we estimate the mean lower limb volume budget to assess the relationship between SFWMT and the export of waters across OSNAP East after accounting for the waters entering the lower limb across the GSR and AB sections (Figure 4).

Using the 6-year OSNAP observations and the GSR observations, we find that the mean lower limb divergence (6.6 ± 0.6 Sv) between the OSNAP East and GSR sections exceeds the mean SFWMT (4.9 ± 1.2 Sv) over the area by about 1.7 ± 1.6 Sv (i.e., R in Equation 4), thus showing that the divergence is supplied primarily by SFWMT and secondarily by other processes represented by the residual term (e.g., mixing). Note that the residual estimated using the 6-year OSNAP data differs from that estimated by Petit et al. (2020), who found that SFWMT nearly balances the lower limb divergence, leaving a much smaller residual. This difference is due to the fact that Petit et al. (2020) used the first 21 months of the OSNAP observations from August 2014 to April 2016. This set of months resulted in a large SFWMT (as there is a winter bias) that matched the mean divergence. In our study, we have chosen six full years of data to avoid that bias.

Comparison of the four reanalyses with the observations reveals that ECCO shows a more realistic relationship between the mean divergence and SFWMT. The ECCO mean divergence (11.1 ± 1.3 Sv) exceeds the SFWMT (6.6 ± 1.4 Sv), leaving 4.5 ± 1.8 Sv as the residual. As such, SFWMT is the primary source for the lower limb volume in ECCO. In contrast, for the other three reanalyses, GloSea5, CGLORS, and SODA, the divergence is far larger than the SFWMT, leading to a residual larger than the SFWMT. Thus, processes other than SFWMT play a dominant role in maintaining the lower limb volume in these three reanalyses. Note that uncertainty in SFWMT

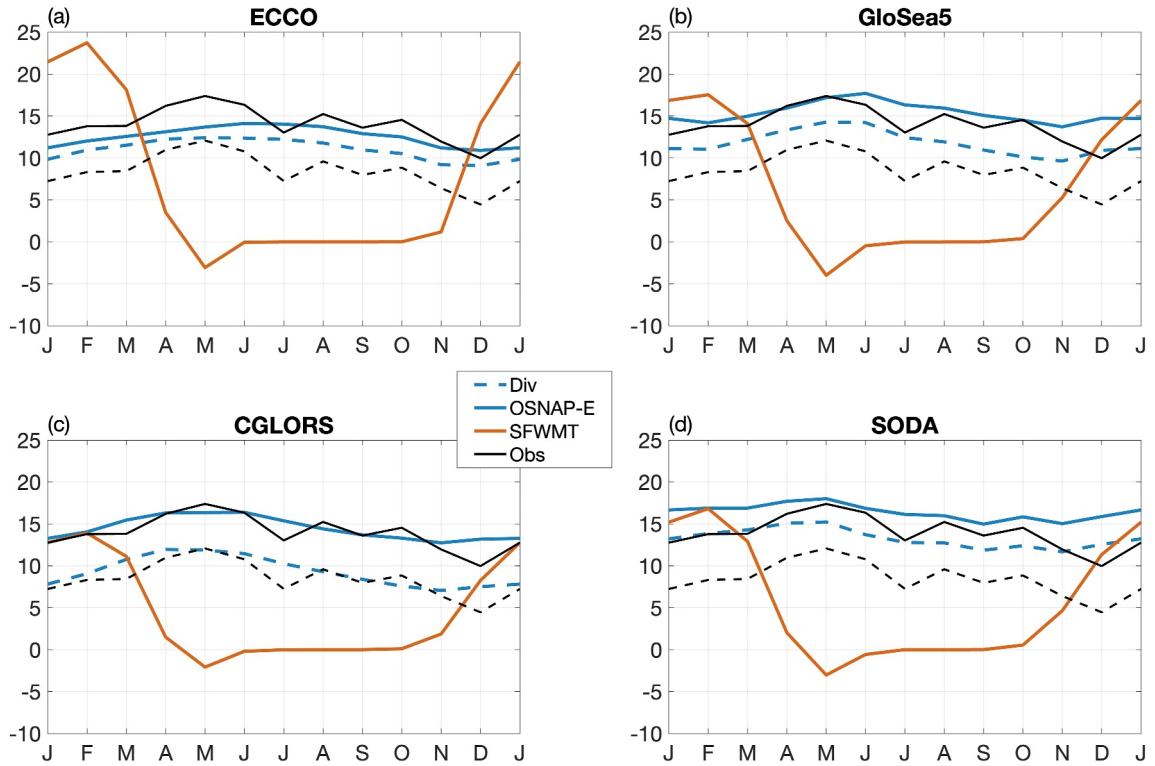

Figure 5. Seasonal cycle of the MOC (solid blue), divergence between OSNAP East and GSR (dashed blue), and surface-forced water mass transformation (solid red) in the eastern subpolar North Atlantic for (a) ECCO, (b) GloSea5, (c) CGLORS, and (d) SODA. The observed MOC and divergence seasonal cycles are superimposed in black for comparison. Note that the observed MOC is calculated using the OSNAP gridded data based on the observed time-mean σ_{MOC}, consistent with the calculation using the reanalyses (see Section 2.3). The unit of the *y*-axis is Sv.

may also arise from the use of different surface flux products (Figure 4 triangles). The calculation using ECCO flux produces the highest SFWMT for the observation and reanalyses, followed by the calculations using ERA5 and NCEP. Such uncertainty may be accounted for when an averaged surface flux field is used.

We now repeat the mean lower limb volume budget for the region between the OSNAP East and AB sections (Figure 4b) for the reanalyses. Here, the divergence is largely balanced by the SFWMT, resulting in a much smaller residual in all reanalyses. Although the AB section is only 300 km south of GSR, the deepest bottom depth of the AB section is over 2,000 m (Figure 1), a dramatic increase from the depth at the GSR section (~500 m). The largely reduced residual is indicative of active water mass transformation due to processes (e.g., mixing and entrainment) along the steep topography within the narrow band between the GSR and AB sections. This is consistent with observations, which show that both the Denmark Strait Overflow Water and Iceland-Scotland Overflow Water transports nearly double their original volume (i.e., at the GSR) along their southward pathways (Dickson et al., 2008; Hansen et al., 2016; Jochumsen et al., 2015; Johns et al., 2021).

3.2. Seasonality

We now assess the seasonality of the OSNAP East MOC and the eastern SPNA SFWMT simulated by the four reanalyses. Using the 6-year OSNAP time series, Fu et al. (2023a) examined the seasonality of the MOC and its relationship with the SFWMT. The authors found that the MOC peaks in spring (May) and reaches a minimum in winter (December). As explained in that study, MOC seasonality is the result of winter production of dense water by SFWMT and Ekman dynamics.

For all four reanalyses, the seasonality of the divergence (dashed blue lines in Figure 5) clearly resembles that of the MOC (solid blue lines in Figure 5). The observed MOC seasonal cycle is reproduced in the reanalyses reasonably well. All reanalyses show a MOC peak in spring (ranging from April to June) and a MOC trough in winter (November). Except for ECCO, the reanalyses exhibit a rapid MOC increase from a winter minimum to

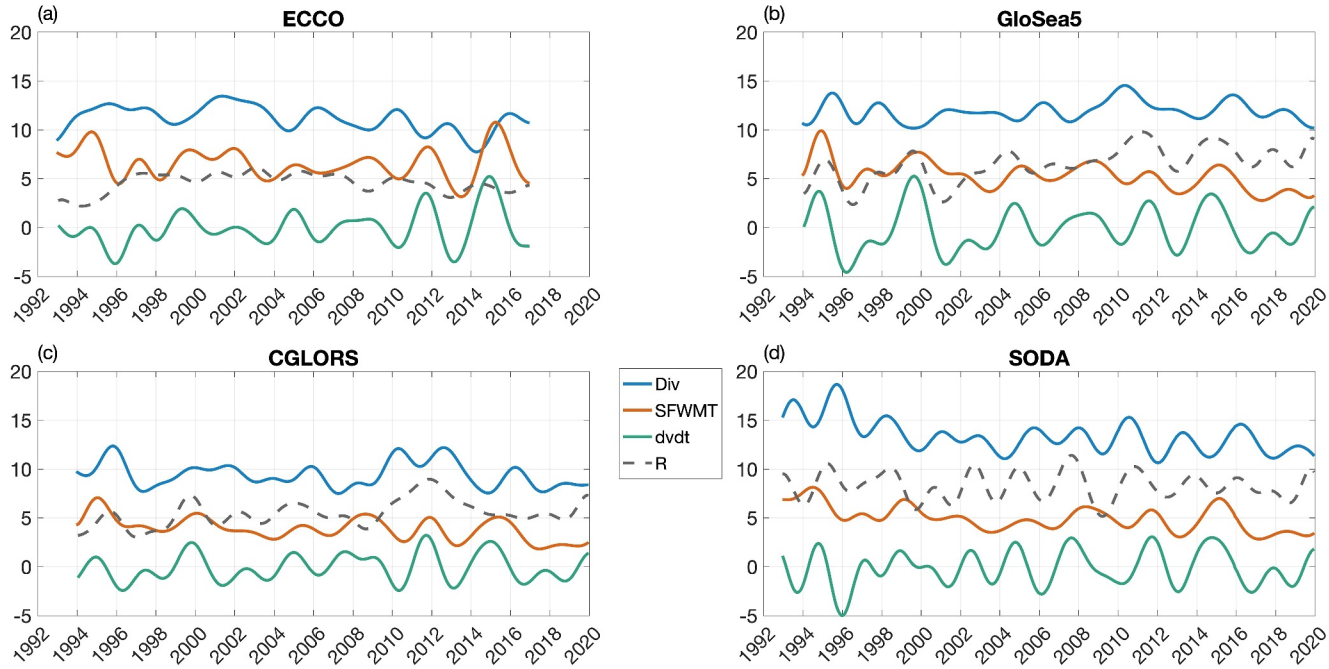

Figure 6. Time series of the divergence (blue), surface-forced water mass transformation (red), volume change (green), and residual (black dashed) between OSNAP East and GSR for (a) ECCO, (b) GloSea5, (c) CGLORS, and (d) SODA. The monthly climatology is first removed from each time series. A 2-year lowpass filter is then applied. The unit of the *y*-axis is Sv.

spring peak and a slow decay for the rest of a year, which is consistent with the observations (Fu et al., 2023a). ECCO, on the other hand, shows a weaker seasonal cycle. Finally, the seasonality of SFWMT in all four reanalyses is consistent with the observations, with a maximum in winter when surface buoyancy forcing is the strongest and a minimum in late spring when restratification of the water column resumes.

In summary, the OSNAP East MOC seasonality in the reanalyses is generally in good agreement with the observed MOC seasonality. The MOC peaks rapidly in spring following the peak of the SFWMT, suggesting that wintertime formation is responsible for the MOC peak in spring consistent with the observations. We add one cautionary note: though the exported waters follow a few months after the SFWMT season, there is no certainty that the exported waters were formed during that particular SFWMT season. As we discuss below, the storage of waters in the lower limb precludes this linkage.

3.3. Interannual Variability

The 6-year OSNAP time series is still relatively short for studying interannual variability. Therefore, we take advantage of the longer time series of the reanalyses to investigate the possible link between SFWMT and the MOC on interannual timescales. First, we calculate each of the components of Equation 3 between OSNAP East and GSR, that is, volume change ($\frac{dVol}{dt}$), divergence, SFWMT, and residual for the layer below the time-mean σ_{MOC} at monthly resolution. We then remove the monthly climatologies from each month and apply a Butterworth lowpass filter with a 2-year filter window to remove high-frequency signals (Figure 6).

At about zero lag, $\frac{dVol}{dt}$ is positively correlated with SFWMT ($R = 0.76$, 0.65, 0.64, and 0.48, for ECCO, GloSea5, CGLORS, and SODA, respectively, and p-value <0.01 for all), whereas it is negatively correlated with the divergence ($R = -0.65$, -0.34, -0.39, and -0.44, and p-value = 0.02, 0.04, 0.02, and 0.005, respectively). Hereafter, the statistics of the reanalyses will be presented in this same order unless stated otherwise. All reanalyses show the expected behavior: the volume increases with enhanced water mass transformation and decreases when there is enhanced divergence. The former relationship is stronger than the latter in all reanalyses.

With about 1 year lag (ranging from 9 to 14 months), the divergence shows the maximum positive correlation with the SFWMT in all reanalyses ($R = 0.56$, 0.22, 0.46, and 0.60, p-value = 0.02, 0.2, 0.01, and 0.005) (Figure S1 in

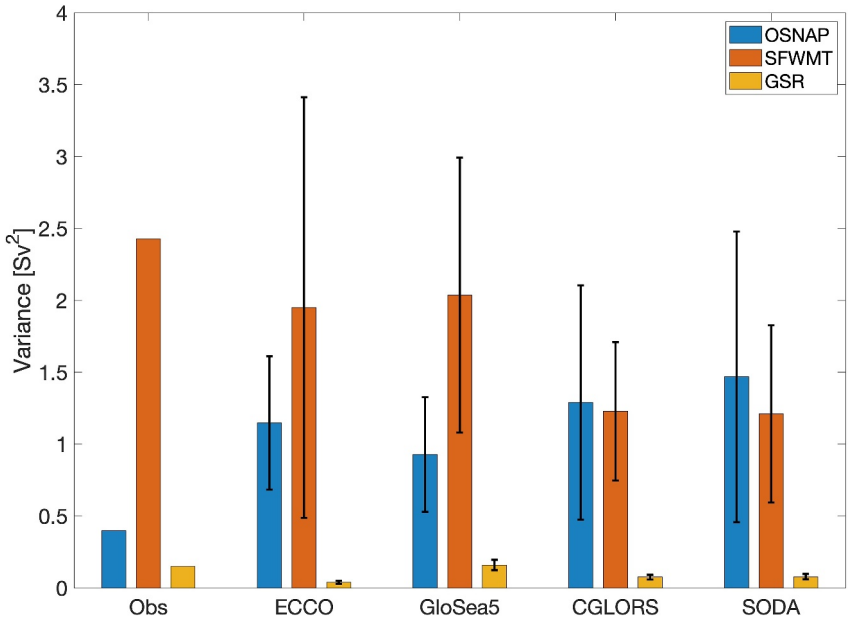

Figure 7. Variances of MOC at OSNAP East (blue), surface-forced water mass transformation (red), and GSR transport (yellow). Variance is calculated based on the annually averaged time series. For the reanalyses, the average of all the variances calculated within each sliding window is presented, and the error bar is the standard deviation of all the variances.

Supporting Information S1). Except for GloSea5, correlations are significant at 95% confidence interval. Note that the variability of the divergence is dominated by MOC variability at OSNAP East ($R \geq 0.95$ between divergence and MOC in all reanalyses). Therefore, this relationship suggests that on interannual timescales newly formed dense water results in an export across OSNAP East with ~1 year delay (As with the seasonal export discussed above, we cannot state with certainty that the waters exported are the same as those formed in the previous year). As a result, the SFWMT explains a significant portion of MOC interannual variability in three of the four reanalyses (i.e., ECCO, CGLORS, and SODA). It is unclear why GloSea5 does not show a significant correlation between SFWMT and the divergence. Given that the same surface flux field is used for CGLORS and SODA and that observed T/S are assimilated in all reanalyses, we are left assuming that the discrepancy is due to specific model dynamics, parameterizations, and assimilation methods.

As for the residual, ECCO has the lowest temporal variability among the four products: the standard deviations for R are 1.2, 1.9, 1.4, and 1.8 Sv for ECCO, GloSea5, CGLORS, and SODA, respectively. Among all reanalyses, ECCO also has the highest correlation coefficients between any pair of variables in Equation 3. These factors together suggest that ECCO, more so than the other reanalyses, has a lower limb volume budget that is largely governed by SFWMT, divergence, and volume change on interannual timescales.

3.4. Representation of Interannual Variances by the Reanalyses

Because the observational temporal span is short relative to that of the reanalyses, we analyze the reanalyses' ability to reproduce the observed interannual variability by comparing variance over time periods that match those of the observations (e.g., 6 years for the MOC and 20 years for the GSR transport). As such, in this section, we compare the (a) variance of the OSNAP East MOC, (b) GSR lower limb transport, and (c) SFWMT of the reanalyses to the same metrics for the observations (Figure 7). To perform the comparison, we calculate an annual time series for each variable using the observations and reanalyses. For a given reanalysis and a given variable (e.g., MOC), we then calculate variance within a sliding window of the same length as the corresponding observations through the annual time series. We compute the mean and standard deviation of variances in all sliding windows and compare with the observation-derived variance. For SFWMT, we also use a 6-year sliding window to be consistent with the OSNAP observations.

In comparison with the observations (0.4 Sv^2), all reanalyses show a much larger variance (1.1 ± 0.5, 0.9 ± 0.4, 1.3 ± 0.8, and 1.5 ± 1.0 Sv^2) in the OSNAP East MOC. The reanalysis-based MOC variance varies strongly

throughout all 6-year windows (as shown by the large standard deviation). However, even accounting for the large variability, the reanalysis-based MOC variance barely overlaps with that of the observations. In contrast, SFWMT variance shows a better agreement between reanalyses (1.9 ± 1.5, 2.0 ± 1.0, 1.2 ± 0.5, and 1.2 ± 0.6 Sv^2) and the observations (2.4 Sv^2), especially when the large standard deviation is considered. ECCO and GloSea5 both produce comparable variance with the observation, whereas CGLORS and SODA produce smaller variance. The reanalyses and the observations agree very well in terms of the GSR transport variance. The much stronger reanalysis variance for OSNAP East MOC suggests two possibilities: 1) The reanalyses actually have substantially larger MOC variance at OSNAP East; and/or 2) the 6 years of OSNAP observations to date does not capture a full spectrum of MOC interannual variability. With the current length of direct MOC observations in the SPNA, it is difficult to identify which option is more plausible.

4. Discussion and Conclusions

In this study, we investigate the relationship between the MOC and SFWMT in the eastern SPNA in the framework of lower limb volume budget. We explore their relationship in the mean on seasonal and interannual timescales using observations and four different reanalyses.

The reanalyses reproduce a consistent mean MOC and SFWMT with the observations. However, the reanalyses generally underestimate the lower limb transport across the GSR section. Our investigation into the mean lower limb volume budget based on the recently available 6-year OSNAP observations reveals that the SFWMT accounts for about 74% of the total transport divergence between the OSNAP East and GSR sections. The remaining 26% is presumably attributed to water mass transformation due to other processes (e.g., mixing). This result is an updated estimate of the mean lower limb volume budget from Petit et al. (2020), whose estimates were constrained by limited data availability at the time of the publication.

Among the four reanalyses, ECCO stands out for producing a more realistic mean volume budget, that is, the SFWMT accounts for a larger portion (60%) of the divergence than the residual term (40%). In comparison, the other three reanalyses (GloSea5, CGLORS, and SODA) produce a higher residual than the SFWMT. As such water mass transformation due to other processes largely balances the divergence in these models. Note that, except for ECCO, which is a dynamically consistent ocean state estimate, the other three reanalyses adopt 3DVar or sequential methods for data assimilation. These methods may introduce artificial sources or sinks of water mass to align the model more closely with observations as acknowledged by Jackson et al. (2019) in a comparative study of reanalyses products. Consequently, the residual term in our analysis of these three products may include erroneous volume fluxes due to the assimilation methods used (Buckley et al., 2023; Evans et al., 2023). As such, readers are advised to interpret the residual term for these models in that context. We also note that the size of the residual term is drastically reduced for the AB section relative to the GSR section for all models particularly for GloSea5 and CGLORS. We attribute these GSR-AB differences in the residual term to physical processes (such as mixing) and/or (for the sequential models) spurious volume changes due to assimilation schemes.

On seasonal timescales, all reanalyses reproduce the observed SFWMT seasonal cycle well. It is encouraging to see that all reanalyses capture the observed annual cycle of the MOC at OSNAP East, that is, they exhibit a peak in spring and a minimum in winter. In particular, GloSea5, CGLORS, and SODA are able to generate the seasonal pattern of the MOC with a rapid increase from the winter minimum to the spring peak and a gradual decrease following the peak in good agreement with OSNAP observations (Fu et al., 2023a). The timing of the MOC peak is consistent with the rapid export of the dense water formed in winter (Le Bras et al., 2020). ECCO on the other hand shows only a weak MOC peak that lasts from spring through summer. A recent study (Han, 2023) based on ECCOr4v3 argues that the MOC decrease from its peak in May to the minimum during the nonconvective months can be well explained by isopycnal heaving over the area between the subtropical and subpolar North Atlantic. This study importantly points to the possible role of adiabatic forcing in driving subpolar MOC seasonal variability. On interannual timescales, three out of four reanalyses (ECCO, CGLORS, and SODA) exhibit significant correlation between the divergence (as well as the MOC) and the SFWMT with the SFWMT leading by about a year (Figure S1 in Supporting Information S1). This relationship confirms the importance of SFWMT in fueling MOC interannual variability. ECCO outperforms the other three reanalyses showing a robust relationship between the different components in the lower limb volume budget that most closely matches the observations.

The reanalyses show a stronger variance in the MOC compared to the observations and comparable variance in the SFWMT. The former mismatch has interesting implications: For the observations, the strong SFWMT

variance but weak MOC variance indicates that only a small portion of the SFWMT variance is transferred into MOC variance. For the reanalyses, in contrast, the MOC and SFWMT variances are of comparable scale. This difference may be due to the fact that the MOC observation is still relatively short and may not cover periods with stronger MOC variability.

Using fidelity to observations as a metric, it is difficult to identify a single reanalysis that outperforms the other reanalyses in all aspects examined in this study. Despite the fact that ECCO produces the weakest mean GSR transport among the reanalyses, it outperforms the other reanalyses in the reproduction of the observed mean lower limb volume budget (i.e., divergence > SFWMT > residual). This performance may be attributed to the fact that ECCO is a dynamically consistent assimilation product that employs the adjoint method (Forget et al., 2015), but we suggest that only as a possibility and leave this matter also for future study. We conclude, however, that of the reanalyses studied here, ECCO is the preferred choice for investigating MOC variability on interannual timescales, while extra caution must be taken regarding the discrepancies mentioned above.

This study sets the framework for understanding the mechanisms driving MOC interannual variability using MOC lower limb volume budget primarily based on ocean reanalysis products. Because the OSNAP project is ongoing, longer records of direct MOC observations will become available soon. The analysis of the 8-year data set will focus on a mechanistic explanation of the observed MOC interannual variability, which will be aided by the use of reanalysis products studied here.

Data Availability Statement

The 2014–2020 OSNAP MOC and gridded velocity products are available in SMARTech Repository via https://doi.org/10.35090/gatech/70342 (Fu et al., 2023b). The ECMWF ERA5 data are available at https://doi.org/10.24381/cds.f17050d7 (Hersbach et al., 2023). The NCEP surface heat and freshwater fluxes are available at the NSF NCAR Research Data Archive via https://doi.org/10.5065/D61C1TXF (Accessed on 2023-12-01; Saha et al., 2014). The Met Office EN4.2.2. g10 data are available at https://www.metoffice.gov.uk/hadobs/en4/ (Accessed on 2023-12-01; Good et al., 2013). ECCOv4r4 is available at https://podaac.jpl.nasa.gov/ECCO (ECCO Consortium). SODA3.15.2 is available at http://www.soda.umd.edu/soda3_readme.htm (Accessed on 2023-12-01; Carton et al., 2018). GloSea5 and CGLORS are available at Copernicus Marine Service via https://doi.org/10.48670/moi-00024 (Accessed on 2023-12-01; Maclachlan et al., 2015; Storto et al., 2016).

Acknowledgments
OSNAP data were collected and made freely available by the OSNAP (Overturning in the Subpolar North Atlantic Program) project and all the national programs that contribute to it (www.o-snap.org). The moorings are part of the global OceanSITES network (http://www.oceansites.org/). EN.4.2.2 data were obtained from https://www.metoffice.gov.uk/hadobs/en4/ and are © British Crown Copyright, Met Office [2023] provided under a Non-Commercial Government Licence. We acknowledge funding from the Physical Oceanography Program of the U.S. National Science Foundation (OCE-1948335).

References

Årthun, M. (2023). Surface-forced variability in the Nordic seas overturning circulation and overflows. *Geophysical Research Letters*, *50*(15). https://doi.org/10.1029/2023GL104158

Bringedal, C., Eldevik, T., Skagseth, Ø., Spall, M. A., & Østerhus, S. (2018). Structure and forcing of observed exchanges across the Greenland-Scotland Ridge. *Journal of Climate*, *31*(24), 9881–9901. https://doi.org/10.1175/JCLI-D-17-0889.1

Buckley, M. W., Lozier, M. S., Desbruyères, D., & Evans, D. G. (2023). Buoyancy forcing and the subpolar Atlantic meridional overturning circulation. *Philosophical Transactions of the Royal Society A: Mathematical, Physical & Engineering Sciences*, *381*(2262). https://doi.org/10.1098/rsta.2022.0181

Carton, J. A., Chepurin, G. A., & Chen, L. (2018). SODA3: A new ocean climate reanalysis. *Journal of Climate*, *31*(17), 6967–6983. https://doi.org/10.1175/JCLI-D-18-0149.1

Desbruyères, D. G., Mercier, H., Maze, G., & Daniault, N. (2019). Surface predictor of overturning circulation and heat content change in the subpolar North Atlantic. *Ocean Science*, *15*(3), 809–817. https://doi.org/10.5194/os-15-809-2019

Dickson, R. R., Meincke, J., & Rhines, P. (2008). In R. R. Dickson, J. Meincke, & P. Rhines (Eds.), *Arctic–subarctic ocean fluxes*. Springer Netherlands. https://doi.org/10.1007/978-1-4020-6774-7

ECCO Consortium, Fukumori, I., Wang, O., Fenty, I., Forget, G., Heimbach, P., & Ponte, R. M. (2023). ECCO central estimate (version 4 release 4). [Dataset]. Retrieved from https://podaac.jpl.nasa.gov/ECCO (Accessed on 2023.12.01)

Evans, D. G., Holliday, N. P., Bacon, S., & Le Bras, I. (2023). Mixing and air-sea buoyancy fluxes set the time-mean overturning circulation in the subpolar North Atlantic and Nordic Seas. *Ocean Science*, *19*(3), 745–768. https://doi.org/10.5194/os-19-745-2023

Forget, G., Campin, J. M., Heimbach, P., Hill, C. N., Ponte, R. M., & Wunsch, C. (2015). ECCO version 4: An integrated framework for non-linear inverse modeling and global ocean state estimation. *Geoscientific Model Development*, *8*(10), 3071–3104. https://doi.org/10.5194/gmd-8-3071-2015

Fu, Y., Lozier, M. S., Biló, T. C., Bower, A., Cunningham, S., Cyr, F., et al. (2023a). Meridional overturning circulation observed by the overturning in the subpolar North Atlantic program (OSNAP) array from August 2014 to June 2020. *Georgia Institute of Technology*. (Accessed on 2023.12.01)

Fu, Y., Lozier, M. S., Biló, T. C., Bower, A. S., Cunningham, S. A., Cyr, F., et al. (2023). Seasonality of the meridional overturning circulation in the subpolar North Atlantic. *Communications Earth & Environment*, *4*(1), 181. https://doi.org/10.1038/s43247-023-00848-9

Good, S. A., Martin, M. J., & Rayner, N. A. (2013). EN4: Quality controlled ocean temperature and salinity profiles and monthly objective analyses with uncertainty estimates. *Journal of Geophysical Research: Oceans*, *118*(12), 6704–6716. https://doi.org/10.1002/2013JC009067

Han, L. (2023). Exploring the AMOC connectivity between the RAPID and OSNAP lines with a model-based data set. *Geophysical Research Letters*, *50*(19). https://doi.org/10.1029/2023GL105225

Hansen, B., Húsgarð Larsen, K. M., Hátún, H., & Østerhus, S. (2016). A stable Faroe Bank Channel overflow 1995–2015. *Ocean Science*, *12*(6), 1205–1220. https://doi.org/10.5194/os-12-1205-2016

Hansen, B., Margretha Húsgar Larsen, K., Malskær Olsen, S., Quadfasel, D., Jochumsen, K., & Østerhus, S. (2018). Overflow of cold water across the Iceland-Faroe Ridge through the western valley. *Ocean Science*, *14*(4), 871–885. https://doi.org/10.5194/os-14-871-2018

Hersbach, H., Bell, B., Berrisford, P., Biavati, G., Horányi, A., Muñoz Sabater, J., et al. (2023). ERA5 monthly averaged data on single levels from 1940 to present. *Copernicus Climate Change Service (C3S) Climate Data Store (CDS)*. https://doi.org/10.24381/cds.f17050d7

Isachsen, P. E., Mauritzen, C., & Svendsen, H. (2007). Dense water formation in the Nordic Seas diagnosed from sea surface buoyancy fluxes. *Deep-Sea Research Part I Oceanographic Research Papers*, *54*(1), 22–41. https://doi.org/10.1016/j.dsr.2006.09.008

Jackson, L. C., Dubois, C., Forget, G., Haines, K., Harrison, M., Iovino, D., et al. (2019). The mean state and variability of the North Atlantic circulation: A perspective from ocean reanalyses. *Journal of Geophysical Research: Oceans*, *124*(12), 9141–9170. https://doi.org/10.1029/2019JC015210

Jackson, L. C., & Petit, T. (2023). North Atlantic overturning and water mass transformation in CMIP6 models. *Climate Dynamics*, *60*(9–10), 2871–2891. https://doi.org/10.1007/s00382-022-06448-1

Jochumsen, K., Köllner, M., Quadfasel, D., Dye, S., Rudels, B., & Valdimarsson, H. (2015). On the origin and propagation of Denmark Strait overflow water anomalies in the Irminger Basin. *Journal of Geophysical Research: Oceans*, *120*(3), 1841–1855. https://doi.org/10.1002/2014JC010397

Jochumsen, K., Moritz, M., Nunes, N., Quadfasel, D., Larsen, K. M. H., Hansen, B., et al. (2017). Revised transport estimates of the Denmark Strait overflow. *Journal of Geophysical Research: Oceans*, *122*(4), 3434–3450. https://doi.org/10.1002/2017JC012803

Johns, W. E., Devana, M., Houk, A., & Zou, S. (2021). Moored observations of the Iceland-Scotland overflow plume along the eastern flank of the reykjanes ridge. *Journal of Geophysical Research: Oceans*, *126*(8), 1–26. https://doi.org/10.1029/2021JC017524

Kanamitsu, M., Ebisuzaki, W., Woollen, J., Yang, S. K., Hnilo, J. J., Fiorino, M., & Potter, G. L. (2002). NCEP-DOE AMIP-II reanalysis (R-2). *Bulletin of the American Meteorological Society*, *83*(11), 1631–1644. https://doi.org/10.1175/bams-83-11-1631

Le Bras, I. A. A., Straneo, F., Holte, J., de Jong, M. F., & Holliday, N. P. (2020). Rapid export of waters formed by convection near the Irminger sea's western boundary. *Geophysical Research Letters*, *47*(3). https://doi.org/10.1029/2019GL085989

Li, F., Lozier, M. S., Bacon, S., Bower, A. S., Cunningham, S. A., de Jong, M. F., et al. (2021). Subpolar North Atlantic western boundary density anomalies and the meridional overturning circulation. *Nature Communications*, *12*(1), 1–9. https://doi.org/10.1038/s41467-021-23350-2

Lozier, M. S., Bacon, S., Bower, A. S., Cunningham, S. A., De Jong, M. F., De Steur, L., et al. (2017). Overturning in the Subpolar north Atlantic program: A new international ocean observing system. *Bulletin of the American Meteorological Society*, *98*(4), 737–752. https://doi.org/10.1175/BAMS-D-16-0057.1

Lozier, M. S., Li, F., Bacon, S., Bahr, F., Bower, A. S., Cunningham, S. A., et al. (2019). A sea change in our view of overturning in the subpolar North Atlantic. *Science*, *363*(6426), 516–521. https://doi.org/10.1126/science.aau6592

Maclachlan, C., Arribas, A., Peterson, K. A., Maidens, A., Fereday, D., Scaife, A. A., et al. (2015). Global seasonal forecast system version 5 (GloSea5): A high-resolution seasonal forecast system. *Quarterly Journal of the Royal Meteorological Society*, *141*(689), 1072–1084. https://doi.org/10.1002/qj.2396

Marshall, J., Jamous, D., & Nilsson, J. (1999). Reconciling thermodynamic and dynamic methods of computation of water-mass transformation rates. *Deep-Sea Research Part I Oceanographic Research Papers*, *46*(4), 545–572. https://doi.org/10.1016/S0967-0637(98)00082-X

Petit, T., Lozier, M. S., Josey, S. A., & Cunningham, S. A. (2020). Atlantic deep water formation occurs primarily in the Iceland basin and Irminger sea by local buoyancy forcing. *Geophysical Research Letters*, *47*(22), 1–9. https://doi.org/10.1029/2020GL091028

Poli, P., Hersbach, H., Dee, D. P., Berrisford, P., Simmons, A. J., Vitart, F., et al. (2016). ERA-20C: An atmospheric reanalysis of the twentieth century. *Journal of Climate*, *29*(11), 4083–4097. https://doi.org/10.1175/JCLI-D-15-0556.1

Rhein, M., Kieke, D., Hüttl-Kabus, S., Roessler, A., Mertens, C., Meissner, R., et al. (2011). Deep water formation, the subpolar gyre, and the meridional overturning circulation in the subpolar North Atlantic. *Deep-Sea Research Part II Topical Studies in Oceanography*, *58*(17–18), 1819–1832. https://doi.org/10.1016/j.dsr2.2010.10.061

Saha, S., Moorthi, S., Wu, X., Wang, J., Nadiga, S., Tripp, P., et al. (2014). The NCEP climate forecast system version 2. *Journal of Climate*, *27*(6), 2185–2208. https://doi.org/10.1175/JCLI-D-12-00823.1

Sherwin, T. J., Griffiths, C. R., Inall, M. E., & Turrell, W. R. (2008). Quantifying the overflow across the Wyville Thomson Ridge into the rockall trough. *Deep-Sea Research Part I Oceanographic Research Papers*, *55*(4), 396–404. https://doi.org/10.1016/j.dsr.2007.12.006

Speer, K., & Tziperman, E. (1992). Rates of water mass formation in the North Atlantic ocean. *Journal of Physical Oceanography*, *22*(1), 93–104. https://doi.org/10.1175/1520-0485(1992)022<0093:ROWMFI>2.0.CO;2

Stendardo, I., Buongiorno Nardelli, B., Durante, S., Iudicone, D., & Kieke, D. (2024). Interannual variability of subpolar mode water in the Subpolar North Atlantic. *Journal of Geophysical Research: Oceans*, *129*(3). https://doi.org/10.1029/2023JC019937

Storto, A., Masina, S., & Navarra, A. (2016). Evaluation of the CMCC eddy-permitting global ocean physical reanalysis system (C-GLORS, 1982-2012) and its assimilation components. *Quarterly Journal of the Royal Meteorological Society*, *142*(695), 738–758. https://doi.org/10.1002/qj.2673

Thomas, L. N., & Shakespeare, C. J. (2015). A new mechanism for mode water formation involving cabbeling and frontogenetic strain at thermohaline fronts. *Journal of Physical Oceanography*, *45*(9), 2444–2456. https://doi.org/10.1175/JPO-D-15-0007.1

Wunsch, C., & Heimbach, P. (2006). Estimated decadal changes in the North Atlantic meridional overturning circulation and heat flux 1993–2004. *Journal of Physical Oceanography*, *36*(11), 2012–2024. https://doi.org/10.1175/JPO2957.1